RESEARCH ARTICLE

Effects of muscle damage on ^{31}phosphorus magnetic resonance spectroscopy indices of energetic status and sarcolemma integrity in young *mdx* mice

Christopher Lopez[1] | Abhinandan Batra[1] | Zahra Moslemi[1] | Andrew Rennick[1] |
Kimberly Guice[1] | Huadong Zeng[2] | Glenn A. Walter[3] | Sean C. Forbes[1]

[1]Department of Physical Therapy, University of Florida, Gainesville, Florida, USA

[2]Advanced Magnetic Resonance Imaging and Spectroscopy Facility, McKnight Brain Institute, University of Florida, Gainesville, Florida, USA

[3]Department of Physiology and Functional Genomics, University of Florida, Gainesville, Florida, USA

Correspondence

Sean C. Forbes, Department of Physical Therapy, University of Florida, Box 100154, UFHSC, Gainesville, FL 32610-0154, USA.
Email: scforbes@phhp.ufl.edu

^{31}Phosphorus magnetic resonance spectroscopy (^{31}P-MRS) has been shown to detect altered energetic status (e.g. the ratio of inorganic phosphate to phosphocreatine: Pi/PCr), intracellular acid–base status, and free intracellular magnesium ([Mg^{2+}]) in dystrophic muscle compared with unaffected muscle; however, the causes of these differences are not well understood. The purposes of this study were to examine ^{31}P-MRS indices of energetic status and sarcolemma integrity in young *mdx* mice compared with wild-type and to evaluate the effects of downhill running to induce muscle damage on ^{31}P-MRS indices in dystrophic muscle. In vivo ^{31}P-MRS spectra were acquired from the posterior hindlimb muscles in young (4–10 weeks of age) *mdx* (C57BL/10ScSn-DMD*mdx*) and wild-type (C57BL/10ScSnJ) mice using an 11.1-T MR system. The flux of phosphate from PCr to ATP was estimated by ^{31}P-MRS saturation transfer experiments. Relative concentrations of high-energy phosphates were measured, and intracellular pH and [Mg^{2+}] were calculated. $^{1}H_2O$-T_2 was measured using single-voxel ^{1}H-MRS from the gastrocnemius and soleus using a 4.7-T MR system. Downhill treadmill running was performed in a subset of mice. Young *mdx* mice were characterized by elevated $^{1}H_2O$-T_2 ($p < 0.01$), Pi/PCr ($p = 0.02$), PCr to ATP flux ($p = 0.04$) and histological inflammatory markers ($p < 0.05$) and reduced ($p < 0.01$) [Mg^{2+}] compared with wild-type. Furthermore, 24 h after downhill running, an increase ($p = 0.02$) in Pi/PCr was observed in *mdx* and wild-type mice compared with baseline, and a decrease ($p < 0.001$) in [Mg^{2+}] and a lower ($p = 0.048$) intracellular [H^+] in damaged muscle regions of *mdx* mice were observed, consistent with impaired sarcolemma integrity. Overall, our findings demonstrate that ^{31}P-MRS markers of energetic status and sarcolemma integrity are altered in young *mdx* compared with wild-type mice, and these indices are exacerbated following downhill running.

KEYWORDS

downhill running, energetics, inflammation, *mdx*, muscle damage, muscular dystrophy

1 | INTRODUCTION

Duchenne muscular dystrophy (DMD) is an X-linked recessive disease caused by a mutation in the dystrophin gene and it affects approximately one in 3500–7250 male births.[1,2] Dystrophin helps to maintain the sarcolemmal membrane integrity, and lack of dystrophin leads to increased susceptibility to muscle damage, inflammation, oxidative stress, and fatigue.[3–6] A commonly used mouse model to study dystrophic muscle is *mdx* mice, with the C57BL/10ScSn-Dmdmdx/J strain being widely utilized.[7,8] This strain is well characterized to have an enhanced muscle inflammatory phase during the early stage of development (3 to 10 weeks old), which is thought to be associated with augmented degeneration and regeneration, followed by a more stable mildly progressing period.[9,10] Consistent with this, at a young age in *mdx* mice, a peak inflammatory phase has been reported[9]; however, the potential metabolic alterations have not been well characterized during this stage.

Both magnetic resonance imaging (MRI) and spectroscopy (MRS) have been widely utilized to identify muscle structural and compositional changes in dystrophic skeletal muscle, including events associated with muscle inflammation, fatty tissue infiltration, and fibrotic changes.[11] Along with structural and composition changes in dystrophic muscle, there is evidence of altered energetics at rest and both during and following exercise.[12–15] In resting dystrophic muscle, ^{31}phosphorus magnetic resonance spectroscopy (^{31}P-MRS) has demonstrated altered concentrations of metabolites associated with ATP synthesis and breakdown reactions (see Equations 1 and 2), including an increased ratio of inorganic phosphate to phosphocreatine (Pi/PCr) and reduced PCr/ATP.[13,15,16]

$$PCr + ADP + H^+ \leftrightarrow ATP + Cr \tag{1}$$

$$ATP \rightarrow ADP + P_i \tag{2}$$

The possible reasons for altered energetic status in dystrophic muscle are poorly understood, including at a young age. Potential factors contributing to the altered energetic status in dystrophic muscle are linked to muscle damage and associated inflammatory processes.[17,18] For example, an increased Pi/PCr and reduced PCr/ATP may be linked to elevated creatine kinase flux due to enhanced processes associated with degeneration and regeneration.[16,19] ^{31}P-MRS is capable of monitoring the transfer of phosphate from PCr to ATP through the creatine kinase reaction using saturation transfer experiments.[20,21] Furthermore, the MR transverse relaxation time constant (T_2) has been associated with inflammatory processes,[22] and, therefore, T_2 can be exploited to determine whether there is a relationship between alterations in ^{31}P-MRS metabolites and inflammation in dystrophic muscle.

Along with monitoring the metabolites associated with ATP production, ^{31}P-MRS has also been utilized to show reduced free intracellular magnesium ([Mg^{2+}])[23] and more alkaline acid–base status[13,15,24] in dystrophic muscle. These changes have been proposed to be linked to compromised sarcolemmal integrity of the muscle cells.[13,15]

Therefore, the purpose of this study was to determine whether ^{31}P-MRS indices of energetics and sarcolemma integrity (i.e. Pi/PCr, intracellular [Mg^{2+}], and acid–base status) are altered in young *mdx* mice during the peak degeneration/regeneration phase compared with wild-type mice, and how these indices are related to muscle T_2. Furthermore, we tested whether alterations in energetics and sarcolemma integrity using ^{31}P-MRS would be further amplified in *mdx* mice after exacerbating muscle damage/inflammation by implementing a downhill running protocol.[6] We hypothesized that metabolic alterations and markers of sarcolemma integrity would be evident with ^{31}P-MRS at a young age in *mdx* mice, further exacerbated with downhill running, and would correspond with elevated muscle T_2.

2 | EXPERIMENTAL

2.1 | Animals

Wild-type (C57BL/10ScSnJ, n = 25) and *mdx* (C57BL/10ScSn-Dmdmdx/J, n = 25) mice were obtained from Jackson Laboratories (Bar Harbor, ME) and were studied between the ages of 4–10 weeks. The mice were housed in an approved Association for Assessment and Accreditation of Laboratory Animal Care facility at the University of Florida (12-h light/dark, 22°C, 42% humidity) and provided food ad libitum. The study was approved by our Institutional Animal Care and Use Committee (IACUC) review board at the University of Florida (Gainesville, FL).

2.2 | General set-up during MR experiments

MRI/MRS experiments were performed using 11.1-T (Bruker Avance with ParaVision 6.0.1) and 4.7-T (Agilent, Santa Clara, CA) MR systems. During all MR experiments, mice were positioned supine on a custom 3D-printed cradle and their lower hindlimbs were scanned. Mice were anesthetized using an oxygen (1 L/min) and isoflurane mixture (3% induction, 0.75%–1% maintenance), and respiration and body temperature were

monitored during all MRI/MRS procedures. A circulated water heating system with flexible water pads was used to keep the mice warm during the scans, and the average rectal body temperature of the mice was measured at 35°C. A subset of mice (10 per group) performed downhill running, and with these mice, MRI/MRS data were collected predownhill and 24-h postdownhill running. The downhill running (14° decline) was performed on a motorized treadmill at a speed of 8–10 m/min, for 30–60 min, as tolerated (Treadmill Simplex II; Columbus Instruments).[6,25]

2.3 | ^{31}P-MRS acquisition

^{31}P-MRS data were acquired at 11.1 T with a 90° block pulse, a repetition time (TR) of 2000 ms, 256 averages, 1024 complex data points, and 8 kHz bandwidth using a dual resonance ^{31}P/^{1}H coil (saddle-shaped oblong coil, 12 x 9 mm; Doty Inc.). ^{31}P-MRS saturation transfer experiments were used to measure the flux of PCr through creatine kinase and indirectly measure the rate of synthesis of ATP (flux).[20,26,27] ^{31}P-MRS saturation transfer experiments were performed with a TR of 13,000 ms, 32 averages, and 8 kHz bandwidth using a calibrated narrow band (110 Hz) single low-power Gaussian pulse (6000 ms irradiation, 1.39 μT) to the γATP peak and also at the mirror site (control), contralateral to the PCr peak.

In addition, after downhill running, localized ^{31}P-MRS data were acquired from a region identified as being damaged by visual inspection of MR images (Rapid Acquisition with Relaxation Enhancement [RARE] sequence; TR = 2500 ms; TE = 7.5 ms; 4–8 slices; RARE factor = 8; FOV ∼ 11 x 11 mm^2, matrix size 192 x 192, effective TE 30 ms). Localization and isolation of ^{31}P-MRS measures in the damaged region were obtained by suppressing the signal outside the region of interest using an optimized field of view (FOV) with adiabatic saturation bands (sech pulses with variable radiofrequency length and amplitudes depending on location, size, and direction). Damaged areas of mouse hindlimbs were isolated using 3–5 saturation bands.

2.4 | ^{1}H-MRI and ^{1}H-MRS acquisitions

T_2-weighted images and ^{1}H-MRS data were acquired at 200.14 MHz with an Agilent (Santa Clara, CA) Direct-Drive console (4.7 T) equipped with a 33-cm horizontal bore and vnmrj 3.1a software. Spin-echo images were acquired from mouse lower hindlimbs (TR: 2000 ms; TE:14 and 40 ms; FOV: 10–15 x 10–15 mm^2; slices: 12; slice thickness: 1 mm; acquisition matrix: 128 x 256). Images and spectra were acquired with a custom-built, 12-mm diameter, 200-MHz ^{1}H solenoid coil. Single-voxel ^{1}H-MRS data (voxel size optimized for the muscle, soleus: 13.7 ± 4.4 mm^3, range 6–24 mm^3; gastrocnemius: 19.3 ± 15.7 mm^3, range 7–50 mm^3) were acquired using Stimulated Echo Acquisition Mode (STEAM; TR: 9000 ms, 16 TEs exponentially spaced from 5 to 200 ms, four phase cycles).

2.5 | Data processing

^{31}P-MRS data were processed in the time domain using jMRUI (software version 5.1) using the AMARES fitting algorithm. ^{31}P-MR spectra for young mice were acquired and only spectra with a PCr-to-noise ratio of 10:1 were used for analysis, as this has been deemed to result in high confidence measures.[21] This criteria resulted in four mice datasets being excluded. The relative phosphate amplitudes of Pi, PCr, and γ-, α-, and β-ATP were determined with estimated starting values and prior knowledge with jMRUI. ^{31}P-MR spectra were zero-filled to 2048 complex data points, 20 Hz line-broadening was applied, and the PCr peak was used as the reference peak (0 ppm). Intracellular [Mg^{2+}] and intracellular pH were calculated as described previously.[28]

The rate of transfer of phosphate from PCr to γ-ATP was estimated by saturation transfer using a pseudo first-order exchange model. The exchange rate constant of PCr with ATP was calculated based on the equation:

$$k = \frac{\left(1 - \frac{Ms}{Mo}\right)}{(T_1')}, \quad (3)$$

where k is a rate constant describing the loss of magnetization due to the exchange of saturated spins between PCr and ATP, and T_1' is the apparent longitudinal relaxation time of PCr. The T_1' of PCr was empirically determined by measuring T_1 using inversion recovery in a subset of mice (five mdx, five wild-type), and no differences ($p > 0.05$) were found between groups (wild-type 1.78 ± 0.23 vs. mdx 1.74 ± 0.09 s); therefore, a T_1' of 1.76 s was used for all calculations. The T_1' pulse sequence was a pseudo 2D inversion recovery with TR = 14,000 ms. This sequence incorporated a calibrated 180° block pulse and a variable delay consisting of 12 points (4, 7.5, 10, 100, 300, 500, 600, 1000, 1500, 2500, 10,000, and 14,000 ms), followed by a 90° block pulse before acquisition (16 signal averages per point). T_1' was determined by exponential fitting of signal intensity with a variable delay. *Ms* is the steady-state PCr signal under γ-ATP saturation, and *Mo* is the PCr signal at its equilibrium value. *Mo* was

measured using the spectrum acquired with the mirror frequency saturation. Following the calculation of k for PCr, the unidirectional flux of ATP synthesis was calculated as the product of k and PCr concentration based on literature values of dystrophic and wild-type mice.[13]

For the ^{1}H$_2$O-T$_2$ calculation of the gastrocnemius and soleus, principal component analysis was performed using the spectroscopic data followed by monoexponential nonlinear curve fitting analysis using in-house software with Interactive Data Language (Exelis, version 8.5), as previously described.[25] T$_2$ was also calculated from the gastrocnemius and soleus (posterior compartment) using the spin-echo images, as previously described.[6,9,25] Briefly, regions of interest representing the posterior compartment muscles were drawn over five axial slices using OsiriX software (Geneva, Switzerland) to calculate signal intensity (SI), and T$_2$ was calculated assuming a single exponential decay curve.[6,9,25]

2.6 | Histology

After completion of the MR acquisitions, the mice were euthanized, and the gastrocnemius and soleus muscles were harvested. Muscles were embedded in paraffin blocks and processed by the pathology core at the University of Florida. Leica microtome was used to section the tissue; 7–10 μm sections were obtained from the midbelly region of the gastrocnemius and soleus muscles. Sections were stained for inflammatory markers, including macrophages using CD45 (Purified Rat Anti-Mouse CD45; BD PharMingen) and F4/80 antibodies (Thermo Fisher Scientific, catalog no. MF-48000, Research Resource Identifier [RRID] AB_10376289). Slides were imaged using a digital camera (Leica Microsystems, Solms, Germany) and analyzed using ImageJ 1.48v (National Institutes of Health) software. The images were manually analyzed by counting the number of CD45+ cells (brown stain). The total number of cells were counted across slices to obtain the number of CD45+ cells as per a given area for each mouse. These cells were then correlated with MRS H$_2$O-T$_2$ measures acquired from the same region (largest girth) of the gastrocnemius muscle.

2.7 | Statistical analysis

Welch's unpaired two-tailed t-test was used to compare *mdx* and wild-type mice. Relationships among measures were correlated using Spearman's analyses. Statistical analysis was performed using MATLAB (R2019a) with Statistics Toolbox (MathWorks, Natick, MA) and GraphPad Prism for Mac OS (version 8.0.0; GraphPad Software, San Diego, CA). For all comparisons, p less than 0.05 was considered significant. Data are reported as mean ± SD in the text and mean ± SEM in the figures.

3 | RESULTS

3.1 | Muscle T$_2$ and energetics in young *mdx* mice at rest

A large sample size of 25 young *mdx* (6 ± 2 weeks) and 25 young wild-type (5 ± 1 weeks) mice with similar ($p = 0.55$) body weight (*mdx*: 19 ± 4, wild-type: 20 ± 4 g) between groups were evaluated using MRI, ^{1}H-MRS, and ^{31}P-MRS of the hindlimbs. In comparison with wild-type mice, young *mdx* mice had longer ($p < 0.01$) ^{1}H$_2$O-T$_2$ of both the gastrocnemius (wild-type 28.2 ± 1.2 vs. *mdx* 31.0 ± 3.4 ms) and soleus (wild-type 27.5 ± 1.8 vs. *mdx* 31.4 ± 3.9 ms) muscles.

Example ^{31}P-MRS spectra acquired at 11.1 T are shown in Figure 1. The ratio of Pi/PCr was elevated ($p = 0.02$) in *mdx* compared with wild-type, while there was a trend ($p = 0.10$) towards a lower ratio of PCr/ATP in *mdx* versus wild-type (Figure 2). Intracellular [Mg^{2+}] was lower ($p < 0.01$) in *mdx* than wild-type, with no significant differences ($p = 0.41$) with intracellular acid–base between *mdx* ([H$^+$] 84.6 ± 6.6 nM; pH 7.07 ± 0.03) and wild-type ([H$^+$] 87.8 ± 9.5 nM; pH 7.06 ± 0.05; Figure 2). Furthermore, the PCr to ATP flux of phosphate was elevated ($p = 0.04$) in young *mdx* compared with wild-type (Figure 3).

3.2 | Effect of downhill treadmill running on MR markers of pathology

After an acute bout of downhill running, *mdx* ^{1}H$_2$O-T$_2$ measured with ^{1}H-MRS increased ($p = 0.047$) in the posterior compartment (gastrocnemius and soleus) of the hindlimbs in *mdx* from predownhill to postdownhill running (pre: 29.3 ± 1.5; post: 31.0 ± 3.7 ms), whereas there was a decrease ($p < 0.01$) in the ^{1}H$_2$O-T$_2$ of wild-type (pre: 27.5 ± 1.1; post: 25.5 ± 2.0 ms). We observed similar findings using MRI-T$_2$ acquired from the spin-echo images, with a tendency for an increase in *mdx* (pre: 28.5 ± 2.1; post: 30.3 ± 3.6 ms; $p = 0.053$) and a decrease in wild-type (pre: 26.5 ± 0.9; post: 24.9 ± 0.9 ms; $p < 0.01$) after downhill running. Also, *mdx* mice presented visually with increased regions of hyperintense signal in the T$_2$-weighted images, indicating damaged areas of the hindlimbs (Figure 4). These regions corresponded with considerably elevated
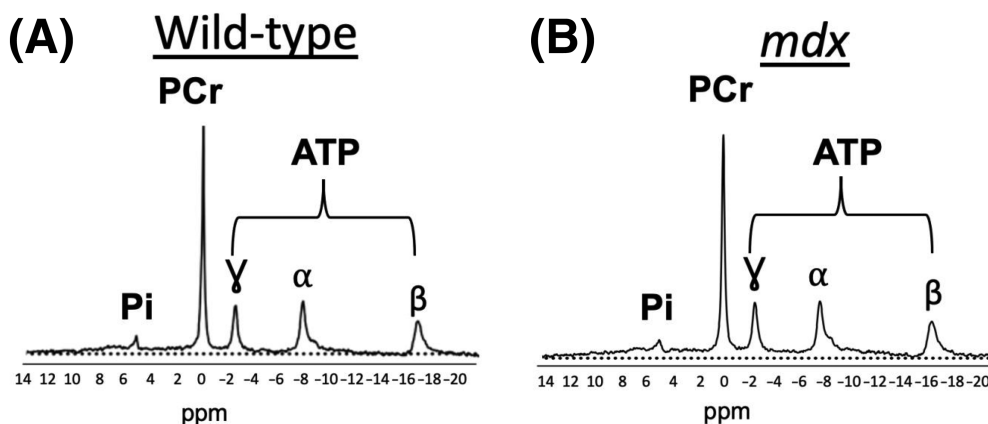
FIGURE 1 Representative spectra acquired using ^{31}P-MRS from the lower posterior hindlimbs of (A) Wild-type and (B) *mdx* mice. Spectra were acquired with TR 2000 ms and 256 averages, and 20 Hz line-broadening applied during postprocessing
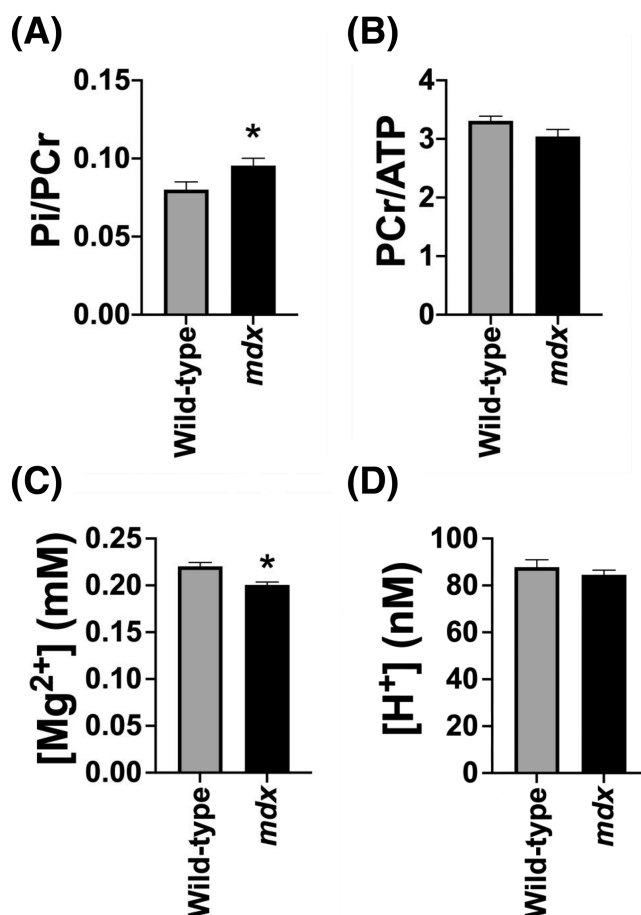

FIGURE 2 ^{31}P-MRS data acquired from the posterior hindlimbs of wild-type (n = 25) and *mdx* (n = 25) mice. (A) Pi/PCr; (B) PCr/ATP; (C) [Mg^{2+}]; and (D) [H$^+$]. [H$^+$], intracellular hydrogen ion concentration; [Mg^{2+}], free intracellular magnesium ion concentration; PCr, phosphocreatine; Pi, inorganic phosphate. *denotes significantly ($p < 0.05$) different from wild-type

($p < 0.001$) ^{1}H$_2$O-T$_2$ values (42.3 ± 7.5 ms) compared with the average ^{1}H$_2$O-T$_2$ value of other muscles examined in dystrophic mice (31.0 ± 3.7 ms).

After downhill running, resting Pi/PCr increased ($p = 0.02$) in both *mdx* (27%; pre: 0.10 ± 0.03; post: 0.12 ± 0.03; Figure 4) and wild-type (31%; pre: 0.08 ± 0.02, post: 0.11 ± 0.03) mice compared with prerunning values. Acid–base status was not significantly altered ($p = 0.89$) in wild-type mice after downhill running ([H$^+$] 88.3 ± 8.1 nM, pH 7.06 ± 0.04) compared with before running ([H$^+$] 87.8 ± 9.5 nM, pH 7.06 ± 0.05). Also,
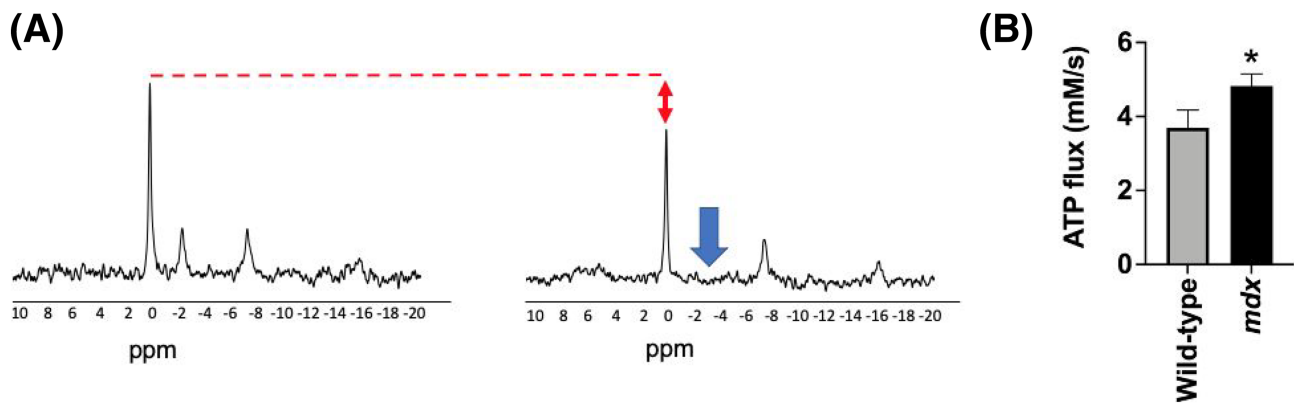
(A)

(B)

FIGURE 3 (A) Example ^{31}P-MRS spectra acquired with saturation of γ-ATP at 11.1 T (blue arrow) and the contralateral mirror chemical shift for reference. (B) The saturation transfer experiments revealed that the transfer rate of phosphate to ATP was greater in young *mdx* (n = 11) than wild-type (n = 7) mice. *denotes significantly different ($p < 0.05$) than wild-type
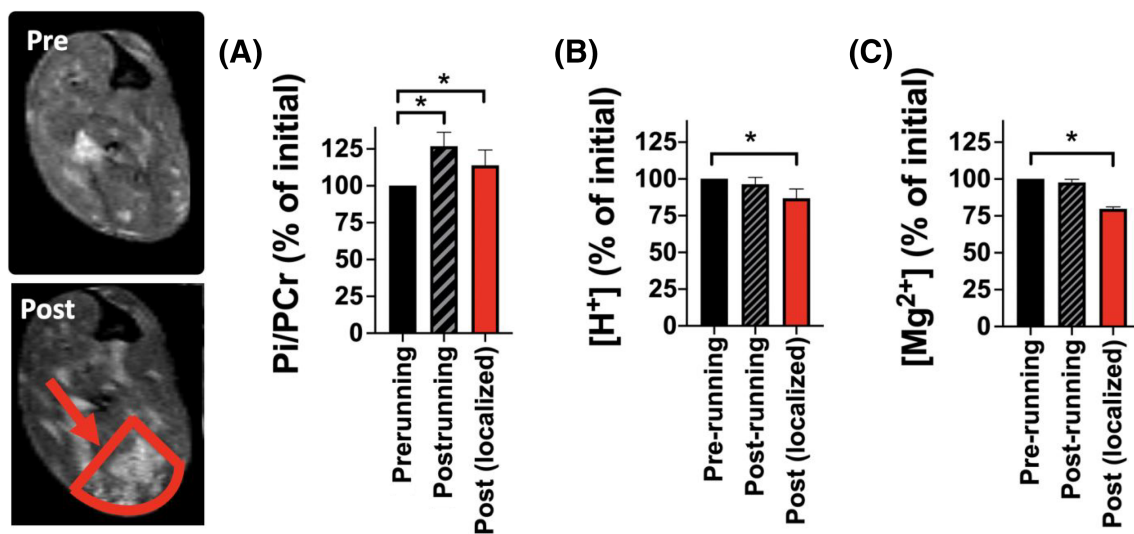

FIGURE 4 Unlocalized ^{31}P-MRS data acquired 24 h after downhill running in the posterior hindlimbs of *mdx* mice (n = 10) were used to compare the percentage change of (A) Pi/PCr, (B) [H$^+$], and (C) [Mg^{2+}] relative to baseline. Also, localized measures of ^{31}P-MRS were acquired from the hyperintense region after downhill running (depicted with the red arrow). *denotes significantly different ($p < 0.05$) than pre

in wild-type mice, intracellular [Mg^{2+}] was not significantly altered ($p = 0.07$) predownhill (0.220 ± 0.012 mM) versus postdownhill (0.242 ± 0.030 mM) running. Unlocalized intracellular [Mg^{2+}] and acid–base status were not altered in the *mdx* or wild-type mice postdownhill compared with predownhill running using nonlocalized ^{31}P-MRS methods (Figure 4). However, in the hyperintense regions of the images, localized ^{31}P-MRS measures were obtained, and in these notably damaged regions, intracellular acid–base status was more alkaline ([H$^+$] 74.0 ± 11.0 nM, pH 7.14 ± 0.07; $p = 0.048$) and intracellular [Mg^{2+}] was decreased (0.155 ± 0.020 mM; $p < 0.001$) in dystrophic muscle postdownhill running compared with nonlocalized measures of dystrophic muscle before exercise, consistent with compromised sarcolemma integrity in the hyperintense regions observed with the T$_2$-weighted images.

3.3 | Correlation between ^{1}H$_2$O-T$_2$, histology, and ^{31}P-MRS measures

Muscle cryosections from *mdx* (n = 10) and wild-type (n = 10) mice were stained with CD 45 and F4/80 antibodies. *Mdx* mice had significantly greater inflammatory markers ($p < 0.001$) compared with wild-type mice (F 4/80 wild-type = 2.8 ± 8.9, *mdx* = 70.0 ± 68.5, CD45 wild-type = 7.1 ± 17.7, *mdx* = 145.2 ± 31.9 cells/mm^2). Furthermore, there was a strong relationship ($\rho = 0.74$) between ^{1}H$_2$O-T$_2$ and CD45 (Figure 5), confirming that ^{1}H$_2$O-T$_2$ is related to muscle damage and inflammatory processes. We also compared ^{1}H$_2$O-T$_2$ among potential ^{31}P-MRS indices of muscle damage at rest with prior exercise and when combined with postrunning data in *mdx* mice. When only prerunning data

were included in the analysis, there were trends for an increase in ^1H_2O-T_2 to correspond with an increase in Pi/PCr ($\rho = 0.31$, $p = 0.25$), decrease in intracellular [H^+] ($\rho = -0.48$, $p = 0.20$), and decrease in intracellular [Mg^{2+}] ($\rho = -0.55$, $p = 0.09$). When the postexercise data were included and the dynamic range of the measures increased, there was a significant relationship between ^1H_2O-T_2 and intracellular [H^+] ($\rho = -0.67$, $p < 0.001$) and intracellular [Mg^{2+}] ($\rho = -0.77$, $p < 0.0001$) in *mdx* mice, while the relationship between ^1H_2O-T_2 and Pi/PCr was not significant ($\rho = 0.34$, $p = 0.11$) (Figure 6).

4 | DISCUSSION

^{31}P-MRS markers of energetic status and sarcolemma integrity were evaluated in the skeletal muscles of young *mdx* mice using unlocalized ^{31}P-MRS measures of the posterior hindlimbs, as well as localized measures of regions that coincided with areas of muscle damage after downhill treadmill running in *mdx* mice. Collectively, our major findings were that (1) indices of energetic status (Pi/PCr and PCr to ATP flux) were altered in young *mdx* mice compared with wild-type, and (2) a marker of muscle sarcolemma integrity (intracellular [Mg^{2+}]) was altered in young *mdx* mice compared with wild-type. Furthermore, ^{31}P indices of sarcolemma integrity (intracellular acid–base status and [Mg^{2+}]) were exacerbated after downhill running in regions of increased T_2 in dystrophic muscle, which were correlated with histological markers of inflammation. Collectively, our findings demonstrate that ^{31}P-MRS detects disease involvement in dystrophic mice at a young age, and these alterations are influenced by muscle damage.
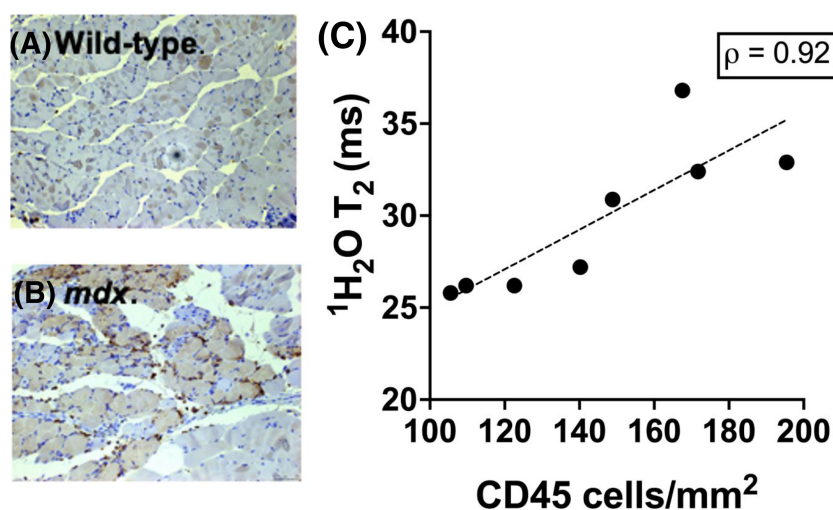

FIGURE 5 Muscle sections were stained for CD45 positive fibers as markers of inflammation in (A) Wild-type and (B) *mdx* mice. (C) The relationship of MR ^1H_2O transverse relaxation time constant (T_2) and CD45 positive fibers in the gastrocnemius of *mdx* mice (n = 8) was examined

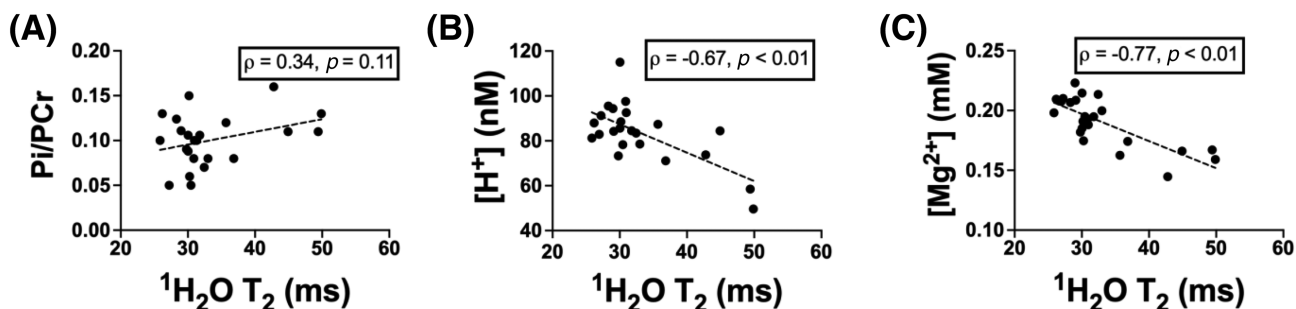**FIGURE 6** Relationship of MR ^1H_2O transverse relaxation time constant (T_2) and (A) Ratio of inorganic phosphate to phosphocreatine (Pi/PCr), (B) Intracellular hydrogen ion ([H^+]), and (C) Intracellular magnesium ([Mg^{2+}]) in *mdx* mice (n = 21). Note that these figures include data acquired postdownhill running (n = 10) to increase the dynamic range of the values. For the subset of mice that did the downhill running (n = 10), only the postdownhill running values were utilized in this analysis (i.e. each mouse has one data point plotted)

4.1 | Energetic status of dystrophic muscle at rest

In this study we observed differences between markers of energetic status in young wild-type and *mdx* mice, and our findings were consistent with the observations of Cole et al.,[13] who observed reduced PCr/Pi and lower PCr/ATP in *mdx* mice at ∼9 weeks of age. Our results were generally comparable with those of Cole et al, although the magnitude of differences between groups was less in our study. For example, Cole et al. observed an altered ratio of Pi/PCr (wild-type: 0.08 vs. *mdx*: 0.13) and PCr/ATP (wild-type: 2.90 vs. *mdx*: 2.52). Similarly, we observed an altered ratio of Pi/PCr (wild-type 0.08 ± 0.02 vs. *mdx* 0.10 ± 0.02), while there was a trend ($p = 0.10$) towards a lower ratio of PCr/ATP in *mdx* (3.04 ± 0.41) versus wild-type (3.31 ± 0.24) in the present study. Also, Heier et al.[16] reported reduced PCr/ATP at 6 weeks of age in *mdx*, but no differences at 8 and 10 weeks; however, that study was limited to three *mdx* mice. Furthermore, Latroche et al.[14] reported increased Pi/PCr and lower PCr/ATP at 12 weeks of age using a different *mdx* strain (*mdx*-4Cv). Similarly, differences in Pi/PCr and PCr/ATP have been observed in Golden retriever muscular dystrophy (GRMD) canines and in humans at rest.[15,29–32] Therefore, dystrophic mice, canine, and human studies have all shown support for an altered ratio of high energy phosphate metabolites at rest, including at a young age. As a result, these measures of energetic status may be valuable markers for evaluating disease involvement and testing therapeutic interventions in dystrophic muscle in future studies. However, the causes of the altered energetics in dystrophic muscle are not well understood.

A potential contributing factor to the increased Pi/PCr levels is increased creatine kinase activity in dystrophic muscle.[19] Consistent with this, we observed greater PCr transfer to ATP in dystrophic muscle using ^{31}P-MRS. In a previous study, creatine kinase activity was observed to be elevated 1.8-fold in the skeletal muscle of 1-month-old *mdx* mice and 3-fold in 3-month-old *mdx* mice compared with wild-type using in vitro measures, and, in that study, this elevated creatine kinase activity coincided with a lower adenylate kinase activity.[19] The contributions and interpretations of the saturation transfer measurements of PCr or Pi to ATP are not completely clear, as the ^{31}P-MRS measures of flux have been observed to overestimate ATP turnover compared with other approaches.[33] Nonetheless, our findings are consistent with elevated creatine kinase activity in *mdx* mice compared with wild-type, and altered relative contributions of the ATP-producing pathways in young *mdx* than wild-type. Unlike the elevated flux we observed in young *mdx* mice in this study, flux was observed to be similar in older *mdx* mice of 16–17 weeks of age.[34,35] Also, the flux of Pi to ATP was observed to be reduced in GRMD canines compared with unaffected controls.[15] This apparent discrepancy may be attributable to the relative stage of the disease studied, with the higher PCr to ATP flux observed in dystrophic mice in this study due to the *mdx* mice being in the peak regenerative/degenerative phase.[9] Future studies are required to gain a better understanding of the causes of the altered flux measures in dystrophic muscle at different stages of the disease.

We observed elevated T_2 and histological inflammatory markers in dystrophic mice, and this indicates that inflammation or factors that alter inflammation also affect energetic status. However, although a relationship between T_2 and ^{31}P-markers of damage were observed, it should be noted that there are other factors than inflammation that could also influence energetic status, such as mitochondria function.[35,36] Also, there may be reduced vascular function and oxygen delivery due to a lack of neuronal nitric oxide synthase,[37] which may be compensated with an increased phosphorylation potential (and increased Pi/PCr).[38]

4.2 | Sarcolemma integrity

Along with monitoring metabolites associated with the ATP-producing/utilization pathways, ^{31}P-MRS has shown reduced free intracellular $[Mg^{2+}]$[23] and more alkaline acid–base status[24] in dystrophic muscle compared with controls in previous studies. The reduced intracellular $[H^+]$ (elevated pH) and free intracellular $[Mg^{2+}]$ is thought to be associated with membrane leakiness, and in some studies two distinct Pi peaks have been resolved, with the interpretation that there is a more alkaline extracellular Pi and a more acidic cytosolic Pi contribution in dystrophic muscle.[15,39,40] Therefore, the elevated pH may reflect a greater concentration of Pi in the extracellular fluid. Intracellular acid–base status may also be altered in dystrophic muscle due to impaired Na^+/H^+ exchange.[12,41] Along with intracellular acid–base status, intracellular $[Mg^{2+}]$ has also been thought to be affected by compromised sarcolemma integrity in dystrophic muscle,[24] and consistent with this, we observed lower intracellular $[Mg^{2+}]$ in *mdx* mice compared with wild-type. Using ^{31}P-MRS to provide an estimate of intracellular $[Mg^{2+}]$ was recently validated by comparison with an independent method using ^{1}H-MRS in dystrophic muscle.[23] In that study, intracellular $[Mg^{2+}]$ was shown to be reduced in a large sample of participants with DMD.

4.3 | ^{31}P-MRS alterations after muscle damage

To further investigate the acute effects of muscle damage and associated inflammation, we implemented an established downhill treadmill running protocol in *mdx* mice.[6]

Several studies have utilized downhill treadmill running in *mdx* mice to exacerbate muscle damage or injury,[6,25] and elevated T_2 has previously been correlated with markers of sarcolemma integrity, such as Evans Blue dye uptake,[6] and shown to have excellent reproducibility (coefficient of

variation of 2.3% for anterior and 3.4% for posterior compartments).[9] In this study, we also observed that downhill treadmill running in *mdx* mice caused an increase in muscle T_2 and visually there were greater regions of hyperintensity in the T_2-weighted images, indicating muscle damage. In these regions, intracellular $[Mg^{2+}]$ and $[H^+]$ were further reduced in *mdx* mice (but not in wild-type), supporting that these measures are altered because of compromised sarcolemma integrity. We also observed an increase in Pi/PCr in both *mdx* and wild-type postdownhill running compared with prerunning. An increase in Pi/PCr was also shown to be elevated after muscle-damaging exercise in humans following a neuromuscular electrical stimulation protocol known to induce muscle damage, as evidenced by prolonged maximal voluntary contraction (MVC) force loss, muscle soreness, and elevated plasma creatine kinase levels.[42] Furthermore, using a protocol consisting of gentle, lengthening contractions with either arms or legs, which was designed to result in mild muscle injury, produced an increase in Pi/PCr that peaked 24 h after exercise.[43] Therefore, Pi/PCr appears to be altered with muscle damage induced by eccentric biased exercise, with this response not only being specific to dystrophic muscle.

4.4 | Limitations and future directions

There are some potential limitations to this study. First, there are inherent limitations of the *mdx* mouse model, including that it is a relatively mild phenotype compared with DMD.[7,8] Future studies may benefit from comparisons with the D2-*mdx* model, which has been reported to be a more severe phenotype and may better mimic the human condition.[44,45] Second, in this study we did not obtain any absolute quantification of metabolites, including ATP and PCr. In addition to the relative concentration of metabolites, it would be valuable to investigate further the absolute quantification of these metabolites. Finally, there are other promising indices derived from ^{31}P-MRS that have been observed in humans with DMD that we were not able to reliably detect in mice, due, presumably, to the small muscle sizes, including two distinct Pi peaks, phosphodiesters (PDE), and phosphomonoesters (PME).[30,32] The effects of muscle damage on the multiple Pi peaks, PDE, and PME may be better studied using a larger animal model or humans.

4.5 | Conclusion

Overall, our findings show that ^{31}P-MRS reveals altered energetic status (Pi/PCr and ATP flux) in young *mdx* mice during the peak degeneration/regeneration phase characterized by enhanced inflammation. Furthermore, exacerbating muscle damage with downhill treadmill running in young *mdx* mice resulted in more alkaline intracellular acid–base status and reduced intracellular $[Mg^{2+}]$ in damaged regions of dystrophic muscle, consistent with compromised sarcolemma integrity. These changes were associated with elevated T_2 and histological markers of inflammation. Therefore, ^{31}P-MRS markers of disease involvement in young *mdx* mice are influenced by muscle damage, and ^{31}P-MRS may be valuable for testing therapeutic interventions aimed at improving energetic status and sarcolemma integrity in dystrophic muscle.

DATA AVAILABILITY STATEMENT

The data that support the findings of this study are available from the corresponding author upon reasonable request.

REFERENCES

1. Romitti PA, Zhu Y, Puzhankara S, et al. Prevalence of Duchenne and Becker muscular dystrophies in the United States. *Pediatrics*. 2015;135(3): 513-521.
2. Hoffman EP, Brown RH, Kunkel LM. Dystrophin: the protein product of the Duchenne muscular dystrophy locus. *Cell*. 1987;51(6):919-928.
3. Petrof BJ, Shrager JB, Stedman HH, Kelly AM, Sweeney H. Dystrophin protects the sarcolemma from stresses developed during muscle contraction. *Proc Natl Acad Sci USA*. 1993;90(8):3710-3714.
4. Kobayashi YM, Rader EP, Crawford RW, et al. Sarcolemma-localized nNOS is required to maintain activity after mild exercise. *Nature*. 2008; 456(7221):511-515.
5. Kim J-H, Kwak H-B, Thompson LV, Lawler JM. Contribution of oxidative stress to pathology in diaphragm and limb muscles with Duchenne muscular dystrophy. *J Muscle Res Cell Motil*. 2013;34(1):1-13.
6. Mathur S, Vohra RS, Germain SA, et al. Changes in muscle T2 and tissue damage after downhill running in mdx mice. *Muscle Nerve*. 2011;43(6): 878-886.
7. McGreevy JW, Hakim CH, McIntosh MA, Duan D. Animal models of Duchenne muscular dystrophy: from basic mechanisms to gene therapy. *Dis Model Mech*. 2015;8(3):195-213.

8. van Putten M, Lloyd EM, de Greef JC, et al. Mouse models for muscular dystrophies: an overview. *Dis Model Mech.* 2020;13(2):dmm043562.

9. Vohra RS, Mathur S, Bryant ND, Forbes S, Vandenborne K, Walter GA. Age-related T2 changes in hindlimb muscles of mdx mice. *Muscle Nerve.* 2016;53(1):84-90.

10. Pratt SJ, Xu S, Mullins RJ, Lovering RM. Temporal changes in magnetic resonance imaging in the mdx mouse. *BMC Res Notes.* 2013;6:262.

11. Strijkers GJ, Araujo ECA, Azzabou N, et al. Exploration of new contrasts, targets, and MR imaging and spectroscopy techniques for neuromuscular disease – a workshop report of working group 3 of the biomedicine and molecular biosciences COST action BM1304 MYO-MRI. *J Neuromuscul Dis.* 2019;6(1):1-30.

12. Dunn JF, Tracey I, Radda GK. A 31P-NMR study of muscle exercise metabolism in mdx mice: evidence for abnormal pH regulation. *J Neurol Sci.* 1992;113(1):108-113.

13. Cole MA, Rafael JA, Taylor DJ, Lodi R, Davies KE, Styles P. A quantitative study of bioenergetics in skeletal muscle lacking utrophin and dystrophin. *Neuromuscul Disord.* 2001;12(3):247-257.

14. Latroche C, Matot B, Martins-Bach A, et al. Structural and functional alterations of skeletal muscle microvasculature in dystrophin-deficient mdx mice. *Am J Pathol.* 2015;185(9):2482-2494.

15. Wary C, Naulet T, Thibaud J-L, Monnet A, Blot S, Carlier PG. Splitting of Pi and other 31P NMR anomalies of skeletal muscle metabolites in canine muscular dystrophy. *NMR Biomed.* 2012;25(10):1160-1169.

16. Heier CR, Guerron AD, Korotcov A, et al. Non-invasive MRI and spectroscopy of mdx mice reveal temporal changes in dystrophic muscle imaging and in energy deficits. *PLoS ONE.* 2014;9(11):e112477.

17. McCully KK, Shellock FG, Bank WJ, Posner JD. The use of nuclear magnetic resonance to evaluate muscle injury. *Med Sci Sports Exerc.* 1992;24(5):537-542.

18. Fulford J, Eston RG, Rowlands AV, Davies RC. Assessment of magnetic resonance techniques to measure muscle damage 24 h after eccentric exercise. *Scand J Med Sci Sports.* 2015;25(1):e28-e39.

19. Ge Y, Molloy MP, Chamberlain JS, Andrews PC. Proteomic analysis of mdx skeletal muscle: Great reduction of adenylate kinase 1 expression and enzymatic activity. *Proteomics.* 2003;3(10):1895-1903.

20. Meyer RA, Kushmerick MJ, Brown TR. Application of 31P-NMR spectroscopy to the study of striated muscle metabolism. *Am J Phys.* 1982;242(1):C1-C11.

21. Meyerspeer M, Boesch C, Cameron D, et al. 31P magnetic resonance spectroscopy in skeletal muscle: Experts' consensus recommendations. *NMR Biomed.* 2020;34(5):e4246.

22. Frisullo G, Frusciante R, Nociti V, et al. CD8+ T Cells in facioscapulohumeral muscular dystrophy patients with inflammatory features at muscle MRI. *J Clin Immunol.* 2011;31(2):155-166.

23. Reyngoudt H, Lopez Kolkovsky AL, Carlier PG. Free intramuscular Mg2+ concentration calculated using both 31P and 1H NMRS-based pH in the skeletal muscle of Duchenne muscular dystrophy patients. *NMR Biomed.* 2019;32(9):e4115.

24. Reyngoudt H, Turk S, Carlier PG. 1H NMRS of carnosine combined with 31P NMRS to better characterize skeletal muscle pH dysregulation in Duchenne muscular dystrophy. *NMR Biomed.* 2018;31(1):e3839.

25. Batra A, Vohra RS, Chrzanowski SM, et al. Effects of PDE5 inhibition on dystrophic muscle following an acute bout of downhill running and endurance training. *J Appl Physiol.* 2019;126(6):1737-1745.

26. Forbes SC, Bish LT, Ye F, et al. Gene transfer of arginine kinase to skeletal muscle using adeno-associated virus. *Gene Ther.* 2014;21(4):387-392.

27. Larsen RG, Befroy DE, Kent-Braun JA. High-intensity interval training increases in vivo oxidative capacity with no effect on Pi→ATP rate in resting human muscle. *Am J Physiol Regul Integr Comp Physiol.* 2013;304(5):R333-R342.

28. Iotti S, Frassineti C, Alderighi L, Sabatini A, Vacca A, Barbiroli B. In vivo ^{31}P-MRS assessment of cytosolic [Mg(2+)] in the human skeletal muscle in different metabolic conditions. *Magn Reson Imaging.* 2000;18(5):607-614.

29. Kemp GJ, Taylor DJ, Dunn JF, Frostick SP, Radda GK. Cellular energetics of dystrophic muscle. *J Neurol Sci.* 1993;116(2):201-206.

30. Younkin DP, Berman P, Sladky J, Chee C, Bank W, Chance B. 31P NMR studies in Duchenne muscular dystrophy: age-related metabolic changes. *Neurology.* 1987;37(1):165-169.

31. Newman RJ, Bore PJ, Chan L, et al. Nuclear magnetic resonance studies of forearm muscle in Duchenne dystrophy. *Br Med J.* 1982;284(6322):1072-1074.

32. Hooijmans MT, Doorenweerd N, Baligand C, et al. Spatially localized phosphorous metabolism of skeletal muscle in Duchenne muscular dystrophy patients: 24-month follow-up. *PLoS ONE.* 2017;12(8):e0182086.

33. Kemp GJ. The interpretation of abnormal 31P magnetic resonance saturation transfer measurements of Pi/ATP exchange in insulin-resistant skeletal muscle. *Am J Physiol Endocrinol Metab.* 2008;294(3):E640-E642.

34. Ryu D, Zhang H, Ropelle ER, et al. NAD+ repletion improves muscle function in muscular dystrophy and counters global PARylation. *Sci Transl Med.* 2016;8(361):361ra139.

35. Percival JM, Siegel MP, Knowels G, Marcinek DJ. Defects in mitochondrial localization and ATP synthesis in the mdx mouse model of Duchenne muscular dystrophy are not alleviated by PDE5 inhibition. *Hum Mol Genet.* 2013;22(1):153-167.

36. Rybalka E, Timpani CA, Cooke MB, Williams AD, Hayes A. Defects in mitochondrial ATP synthesis in dystrophin-deficient mdx skeletal muscles may be caused by complex I insufficiency. *PLoS ONE.* 2014;9(12):e115763.

37. Thomas GD, Victor RG. Nitric oxide mediates contraction-induced attenuation of sympathetic vasoconstriction in rat skeletal muscle. *J Physiol.* 1998;506(Pt 3):817-826.

38. Wilson DF. Factors affecting the rate and energetics of mitochondrial oxidative phosphorylation. *Med Sci Sports Exerc.* 1994;26(1):37-43.

39. Hogrel J-Y, Wary C, Moraux A, et al. Longitudinal functional and NMR assessment of upper limbs in Duchenne muscular dystrophy. *Neurology.* 2016;86(11):1022-1030.

40. Wary C, Azzabou N, Giraudeau C, et al. Quantitative NMRI and NMRS identify augmented disease progression after loss of ambulation in forearms of boys with Duchenne muscular dystrophy. *NMR Biomed.* 2015;28(9):1150-1162.

41. Gerhalter T, Gast LV, Marty B, et al. 23Na MRI depicts early changes in ion homeostasis in skeletal muscle tissue of patients with duchenne muscular dystrophy. *J Magn Reson Imaging.* 2019;50(4):1103-1113.

42. Foure A, Wegrzyk J, Le Fur Y, et al. Impaired mitochondrial function and reduced energy cost as a result of muscle damage. *Med Sci Sports Exerc.* 2015;47(6):1135-1144.

43. McCully KK, Argov Z, Boden BP, Brown RL, Bank WJ, Chance B. Detection of muscle injury in humans with 31P magnetic resonance spectroscopy. *Muscle Nerve.* 1988;11(3):212-216.

44. Hammers DW, Hart CC, Matheny MK, et al. The D2.mdx mouse as a preclinical model of the skeletal muscle pathology associated with Duchenne muscular dystrophy. *Sci Rep.* 2020;10(1):14070.

45. Coley WD, Bogdanik L, Vila MC, et al. Effect of genetic background on the dystrophic phenotype in mdx mice. *Hum Mol Genet.* 2016;25(1):130-145.